Final Draft
of the original manuscript:

Mohedano, M.; Serdechnova, M.; Starykevich, M.; Karpushenkov, S.;
Bouali, A.C.; Ferreira, M.G.S.; Zheludkevich, M.L.:

**Active protective PEO coatings on AA2024: Role of voltage on
in-situ LDH growth**

Active protective PEO coatings on AA2024: role of voltage on in-situ LDH growth

M. Mohedano[1,2*], M. Serdechnova[1], M. Starykevich[3], S. Karpushenkov[4], A. C. Bouali[1], M.G.S. Ferreira[3], M.L. Zheludkevich[1,3]

[1] Institute of Materials Research, Helmholtz-Zentrum Geesthacht, Max-Planck-Straβe 1, 21502 Geesthacht, Germany

[2] Departamento de Ciencia de Materiales, Facultad de Ciencias Químicas, Universidad Complutense, 28040 Madrid, Spain

[3] Department of Materials and Ceramic Engineering, CICECO – Aveiro Institute of Materials, University of Aveiro, 3810-193 Aveiro, Portugal

[4] Belarusian State University, Faculty of Chemistry, 4, Nezavisimosti avenue, 220030, Minsk, Belarus

*Corresponding author. Tel: +494152871956+; Fax:+ 494152871960

E-mail: mmohedan@ucm.es

Abstract

Four voltage-controlled plasma electrolytic oxidation (PEO) coatings were developed on AA2024 aluminum alloy at 350 V, 400 V, 450 V and 500 V. Zn–Al LDH layer was *in situ* grown and loaded with corrosion inhibitor (vanadate) on the coatings to provide active protection to the PEO layers. The structure, morphology and composition of PEO coatings without and with LDH-NO_3 and LDH-VO_x were investigated using SEM, EDS, XRD and GDOES. Coatings formed at higher voltages (thicker and more stable) reveal a decrease of LDH flakes on the surface. The corrosion behavior and the effectiveness of LDH formation and inhibitor intercalation were also studied. Electrochemical impedance spectroscopy and scanning vibrating electrode techniques have shown a remarkable increase in the corrosion resistance of the LDH-inhibitor treated sample in comparison with PEO coated AA2024 specimen.

Keywords

PEO; Active protection; LDH; Corrosion.

1. Introduction

Ceramic-like coatings formed with plasma electrolytic oxidation (PEO) make possible indeed strong improvement of the mechanical properties and corrosion resistance of Al alloys which can therefore be used more widely, hence providing low weight structures [1,2]. PEO process takes place in environmentally friendly dilute electrolytes and involves anodic polarization of the Al alloy to voltages above the dielectric breakdown causing plasma micro-discharges across the growing oxide. The final coating is mainly composed of the substrate metal oxide but also more complex oxides and compounds which involve the components presented in the electrolyte [3,4].

Recent advances for PEO coated Al alloys are focused on the possibility to create surfaces that respond to the raising demand of multifunctional applications. Tailored PEO coatings can be achieved in one step process, adjusting the electrolyte composition [5-7] and process parameters [8,9], or in two step processes with the use of post-treatments. Existing post-treatments for PEO include immersion in phosphate, silicate or borate-containing solutions and other approaches such as sol–gel, polymers, etc. [10-12]. All these treatments aim at improving the long term corrosion resistance of PEO coatings, which are prone to failure due to porous structure that allows fast ingress of corrosive species. Improving barrier does not always ensure a long life in service because of formation of scratches, cracks and other exploitation induced defects. The only way to avoid propagation of corrosion in such defects is to use active inhibition concepts which are unfortunately not offered by the above mentioned sealings.

A novel approach in this direction could be the presence of inhibitor species in the coating that suppress the corrosion activities when the substrate is in contact with an aggressive environment [13-16]. Up to date it is a challenge to create functional PEO-based surfaces that can provide active protection showing a "self-healing" response to defects arising during service and only few studies, which are focused only on Mg alloys, are available. Gnedenkov et al. obtained an improvement of the corrosion properties for PEO coated Mg alloy (MA8) after immersion post-treatments in solution containing inhibitor species (8-hydroxyquinoline) [17]. It was also shown in author´s previous work that immersion post-treatments using Ce(III) nitrate might activate the "self-healing" properties of PEO coated AM50 Mg alloy due to the stabilization of the inner barrier PEO layer by the released RE cations [18]. In the particular case of aluminum alloys, Oleinik et al. conducted investigations on PEO coated

AMg-5 and D16 Al alloys and found an improvement in the corrosion resistance after immersion post-treatments with solutions containing inhibitors (IFKhAN-25 and IFKhAN-39) [19,20]. However, the sealing of PEO coatings with corrosion inhibitors does not allow the release *on demand* when corrosion processes starts: leaching takes place during all the time of immersion in the electrolyte due to the concentration gradient. A further step in the incorporation of inhibitors into PEO coatings is the recent work by Sun et al. using halloysite nanotubes (HNT) loaded with benzotriazole (BTA). An improvement of the corrosion resistance was achieved for the coated AM50 Mg alloy due to a prolonged inhibition effect [21].

The use of micro and nanocontainers can improve the effective incorporation of inhibitors that can provide active protection with a triggered release [22]. Among different approaches to encapsulate inhibiting compounds [23-25], layered double hydroxides (LDHs) have been successfully proved to enhance the corrosion behavior of bare Al alloys [26-28] as well as anodized surfaces [29,30]. The LDH structure consists of layers of mixed metal hydroxides separated by layers of anions and water [31,32]. The protective mechanism of LDH loaded with inhibitive anions is based on the anion-exchange reaction induced by particular triggers such as pH increase or presence of aggressive species (typically chlorides) in the solution [33].

In recent author´s work, the concept of inhibitor-containing LDH-based post treatment for sealing the PEO layers was proven for the first time [34]. However, the suitability of LDH formation for PEO coatings is not clear due to the complex composition and morphology of these coatings, including several types of aluminum oxides. The present study aims at systematic understanding the effect of PEO properties on the LDH sealing and correlation of PEO structure/composition with LDH growth mechanism on the 2024 aluminum alloy. This alloy is widely applied in the aeronautics and aerospace sectors due to its low density and good mechanical properties, but the presence of Cu rich precipitates compromises the corrosion resistance and surface modification is commonly used to fulfill the requirements in service [35].

2. Experimental

2.1. Material

The composition of the 2024-T3 aluminum alloy in wt.% is: 3.8–4.9 Cu, 0.5 Fe, 0.1 Cr, 1.2–1.8 Mg, 0.3–0.9 Mn, 0.5 Si, 0.15 Ti, 0.25 Zn, 0.15 others and Al balance. The samples were cut from sheets into specimens of 20 mm $\times$ 30mm $\times$ 2mm dimensions, ground to P1200 silicon carbide abrasive paper, rinsed in distilled water and methanol and dried in warm air.

2.2. Surface treatment based on PEO

The PEO processing was conducted at constant voltage using four different sets of conditions (350 V, 400 V, 450 V, 500 V) during 15 min. A pulsed DC power supply with a pulse ratio of t_{on}: t_{off}=1ms:9ms was used and the electrolyte (10 g L^{-1} Na_2SiO_3, 2g L^{-1} NaOH and 10g L^{-1} $Na_2H_2P_2O_7$ dissolved in deionized water) was continuously stirred during the treatment and kept at 20 $\pm$ 2 °C using a water cooling system. The counter-electrode was made of stainless steel. After PEO treatment, the specimens were rinsed in deionized water and dried in warm air.

2.3. Post-treatment based on LDH growth

Zn-Al LDH-nitrate (LDH-NO_3) was synthesized on the surface of PEO treated AA2024 alloy using 100 ml of aqueous $Zn(NO_3)_2 \cdot 6H_2O$ (0.1 M) and NH_4NO_3 (0.6 M). The pH of the original solution was adjusted to 6.5 using 1% ammonia [34] and solution was warmed up to 95 °C. The specimens were immersed in the solution for 30 minutes under continuous stirring in order to form LDH and then rinsed using deionized water and dried in air at room temperature.

2.4. Inhibitor intercalation

Zn-Al LDH-vanadate (LDH-VO_x) was obtained via anion exchange reaction by immersion of PEO-LDH parental samples in 100 ml of 0.1 M $NaVO_3$ solution (pH adjustment to 8.4 using 1M NaOH) during 30 min at 50 °C [34]. After the anion exchange reaction, the specimens were rinsed with deionized water and dried in air at room temperature.

2.5. Characterization

Specimens were examined in plan and cross-section views using a Tescan Vega3 SB scanning electron microscope (SEM) equipped with an energy dispersive X-ray (EDX) spectrometer. Coating cross-sections were ground through successive grades of SiC paper and polished to 1 μm diamond finish.

Phase composition was examined by X-ray diffraction (XRD), with a PANalytical X'Pert Powder diffractometer (Ni-filtered Cu Kα radiation, 0.02^o step size, ~1.5 s dwell time) at room temperature.

Glow discharge optical emission spectroscopy (GDOES) depth profile analysis of the coatings was conducted with a HORIBA GD-Profiler 2 (4 mm anode, 650 Pa operating pressure and 30 W power).

2.6. Electrochemical behavior

Electrochemical impedance spectroscopy was performed in a naturally aerated 0.5 wt.% NaCl solution at room temperature (22 °C) up to 3 days of immersion. Measurements were conducted with a Gill AC computer-controlled potentiostat using a conventional three-electrode cell, employing a platinum mesh counter electrode, a silver/silver chloride reference electrode (Ag/AgCl) and the working electrode was the test material (exposed area 0.5 cm^2). All measurements were repeated twice with good reproducibility.

Scanning vibrating electrode technique (SVET) measurements were conducted using Applicable Electronics Inc. (USA) instrumentation and controlled with the ASET-LV4 software (ScienceWares, USA). The spherical black platinum vibrating microelectrode (with diameter of 20–30 μm) vibrated with 30 μm amplitude (both normal and parallel directions to the sample surface) at an average distance of 100 μm above the surface. The free *QuickGrid* (version 1.2) software was used for presentation of SVET maps.

3. Results and discussion

3.1. Coating characterization

Figure 1 shows the plan view and cross-section scanning electron micrographs of AA2024 coated by PEO at different voltages (350 V-500 V). PEO process conducted under 350 V

forms a very thin oxide layer where the polishing marks are still visible. The presence of bigger pores (indicated in the Fig. 1 a) is associated with secondary phases in the alloy (several intermetallics: AlCuMg, AlCuMnFeSi [36]) that have a different behavior relative to the matrix during the oxidation process [37]. This type of heterogeneities, showing a negative effect on the morphology of the porous oxide layer, is common for conventional anodizing [38,39] but PEO process can overcome this disadvantage in most of the cases due to the higher energy input [10]. However, at low voltages (350 V) the presence of intermetallic leads to some irregularities in the oxide layer like in the case of conventional anodizing. For the particular low voltage treatment (PEO-350 V) in this work there are two factors responsible for the formed defects: i) electrical parameters: the combination of relative low voltage and low duty cycle produces micro-discharges with lower intensity that have been reported to develop thin layers [40] ii) surface preparation: it only involved mechanical grinding before PEO processing and even it is generally considered as non-critical for PEO.

An increase in the voltage (Fig. 1 c,e,g) eliminates the defects related to secondary phases and the typical surface morphology of plasma electrolytic oxidation layers becomes clearer. This is characterized by pores and micro-cracks on the surface at the sites of the discharge channels due to the gas evolution through the molten oxide material during the PEO process and thermal stresses, respectively [3]. It can be observed that higher voltages decreases the pore density whereas the pore size increases, which agrees with other works [41,42], with a maximum pore size of 3 μm and 9 μm for PEO-350 V and PEO-500 V respectively.

The cross-sectional examination reveals important differences regarding the thickness of the coatings. The PEO treatment performed at 350 V (Fig. 1 b) results in a very thin coating (about 1 μm) that is not clearly visible at the used magnification. An increase of 50 V in the applied voltage slightly increases the thickness of the coating (less than 2 microns). A more significant change is revealed for coatings developed under higher voltages (thickness: ~ 6±3 μm for PEO-450 V and 13±4 for PEO-500 V), that visually corresponds during the PEO process to the presence of strong sparks over the entire surface (Fig.1 d,f,h). This is in agreement with previous studies reporting that electrical parameters play a crucial role in the microstructure of the final PEO coatings, and in particular higher energy inputs (voltage or current density) leads to thicker coatings [41,43]. Coatings formed under voltages higher than 400 V, show the typical structure of PEO coatings produced in electrolytes containing phosphates using DC pulse electrical regime, which consists of a two-layers coating (outer porous and inner barrier) layer with a pore band between them [44].
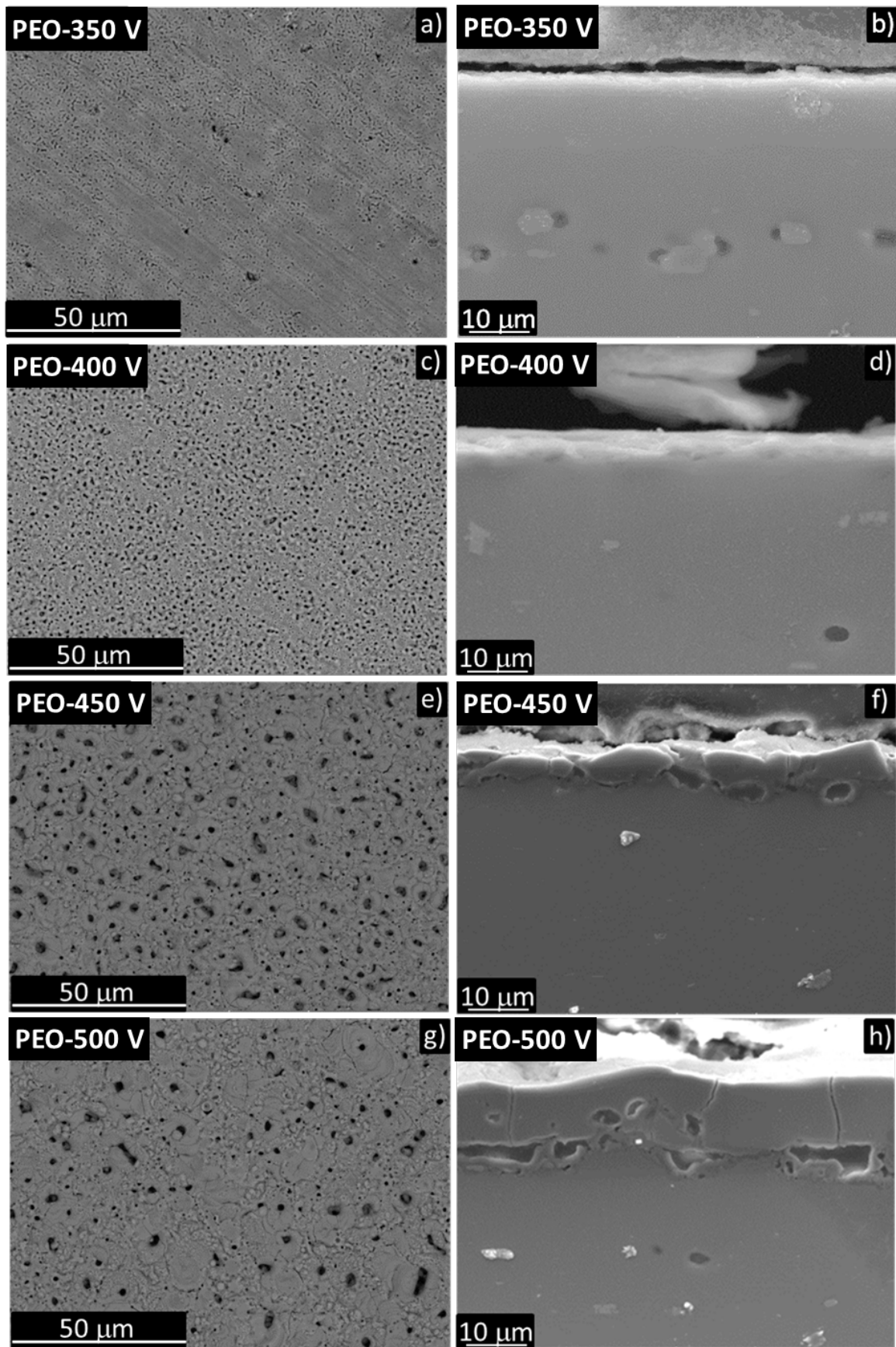
Figure 1

Figure 2 depicts a detailed morphology of PEO coatings at different voltages before and after modification with post-treatments based on LDH-NO$_3$. The typical flake-like LDH structure [33] can be clearly observed for PEO-350 V-LDH (Fig.2 b). The size of the hexagonal flakes is estimated to be about 1-2 μm (which is in a good agreement with previously published [34]) and they are covering the whole PEO treated surface. This type of LDH morphology and the sealing effect is also detected for PEO-400 V-LDH (Fig.2 d). However, for higher voltages there is a drastic decrease of the density of LDH-like flakes, so that for PEO-500 V-LDH it is difficult to distinguish them (Fig.2 h). This fact is associated with the mechanism of *in situ* Zn-Al LDH grown which strongly depends on the amount of Al(OH)$_2^+$ cations available from the material. Unlike co-precipitation synthesis, where the source of Al(OH)$_2^+$ cations required is supplied by an external source [33], for the *in situ* grown method used in this work, the source of Al^{3+} cations proceeds directly from the coated material and is determined by the individual characteristic of PEO coatings as can be clearly observed in Figure 2. The surface appearance persists after the loading of LDH with vanadates anions (images not shown) as it was previously reported in recent author´s work [34].
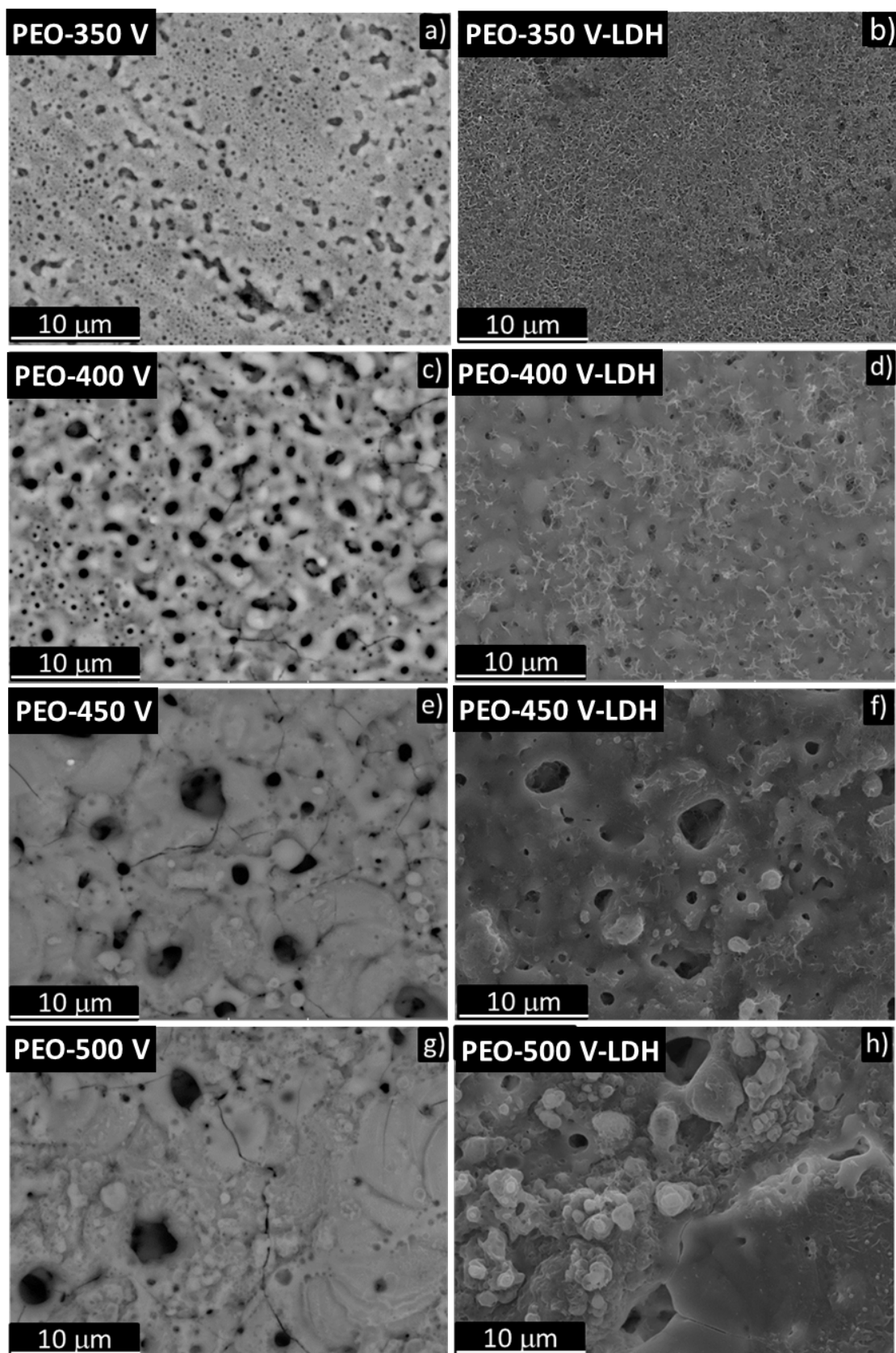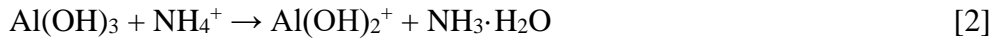
Figure 2

As it was previously suggested, Zn-Al LDH synthesis could be explained via following chemical reaction [45]:

$$Al_2O_3 + 3H_2O \rightarrow 2Al(OH)_3 \qquad [1]$$

$$Al(OH)_3 + NH_4^+ \rightarrow Al(OH)_2^+ + NH_3 \cdot H_2O \qquad [2]$$

$$Zn(OH)^+ + Al(OH)_2^+ + 2NO_3^- \rightarrow LDH\text{-}NO_3 \qquad [3]$$

Due to the porous structure, there are two sources that can provide $Al(OH)_2^+$ cations: i) the metal matrix, due to the electrochemical interactions in contact with the solution used for LDH synthesis and ii) the degradation of Al_2O_3-based PEO coatings. The first one (cations proceeding from the matrix) is determined by the tortuosity of the coating [46]. The tortuosity describes the accessibility of the electrolyte to the metal surface and can be used as a factor, quantifying the interlinking of pores, channels, cracks, etc. (higher tortuosity is, lower accessibility of electrolyte is observed, $\tau = 1$ for an infinitely small layer thickness). Taking into account the coatings cross-section (Fig.1) and plan view after the post-treatments (Fig.2), it can be concluded that the number and size of LDH flakes on the surface of PEO coatings decreases for thicker coatings. The coating barrier effect makes it difficult the penetration of the solutions used for LDH synthesis to the substrate through the pores and therefore the contact with the AA2024 matrix is limited.

The cations availability from the PEO coating (second source of $Al(OH)_2^+$) is mainly controlled by the chemical stability of the oxide layer. It is already known that PEO coatings developed at higher voltages show more stable phases (α-Alumina and mullite) due to the high temperature of the microdischarges achieved during the coating process and they are more difficult to dissolve (compared to γ-Al_2O_3 or amorphous Al_2O_3) [41]. The XRD results on the PEO specimens treated at different voltages confirm this hypothesis (Fig. 3). PEO coatings formed under 350 V and 400 V shows very strong peaks of Al proceeding from the substrate, a hump at low angle (related to amorphous phase) and gamma alumina peaks. Increasing the voltage, the peaks corresponding to the substrate become less intensive and practically negligible in the case of PEO-500 V. Also for coatings developed using 450 V and 500V alumina peaks can be detected. This mixture of α-Al_2O_3, γ-Al_2O_3 is more stable (in comparison with coatings form of γ-Al_2O_3) and let it difficult to release of $Al(OH)_2^+$ to form LDH flakes.
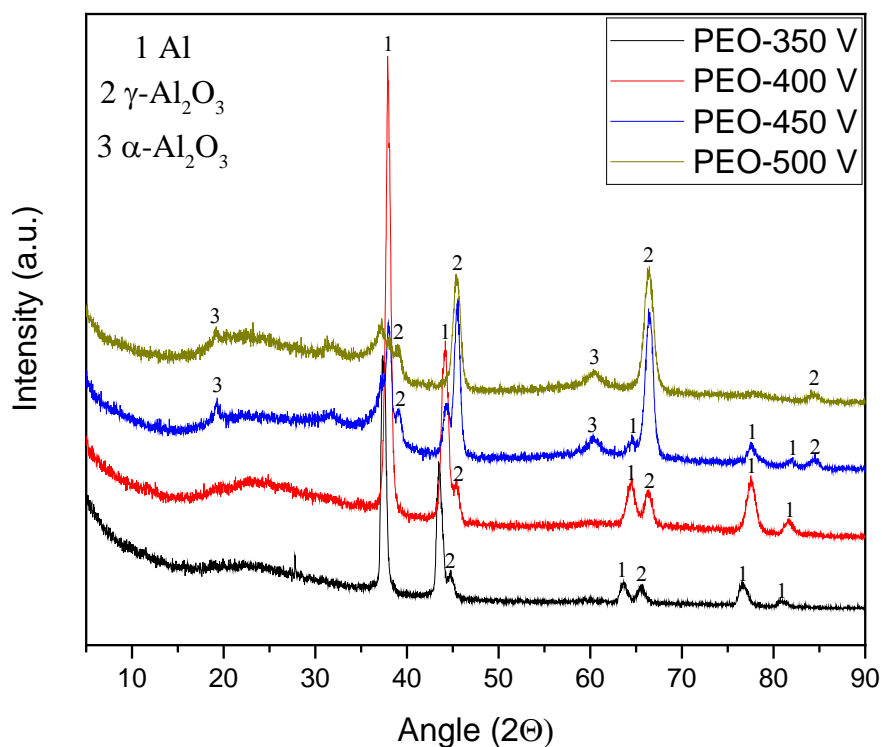
10

Figure 3

Figure 4 depicts the XRD patterns of PEO coated AA2024 at different voltages (350 V–500 V), covered with LDH before (LDH-NO$_3$) and after inhibitor intercalation (LDH-VO$_x$). For PEO developed at lower voltages (350 V and 400 V) well-defined peaks at 9.64° and 19.34° are detected that corresponds to the characteristic (003) and (006) reflections of LDHs intercalated with NO$_3^-$. After the anion exchange reaction with vanadate species, a shift can be observed in those peaks corresponding to the increase of intergallery distance and successful formation of LDH-VO$_x$ [47]. In the case of higher voltages, due to the lower amount of LDH and smaller size of the flakes on the surface, the XRD peaks are negligible.
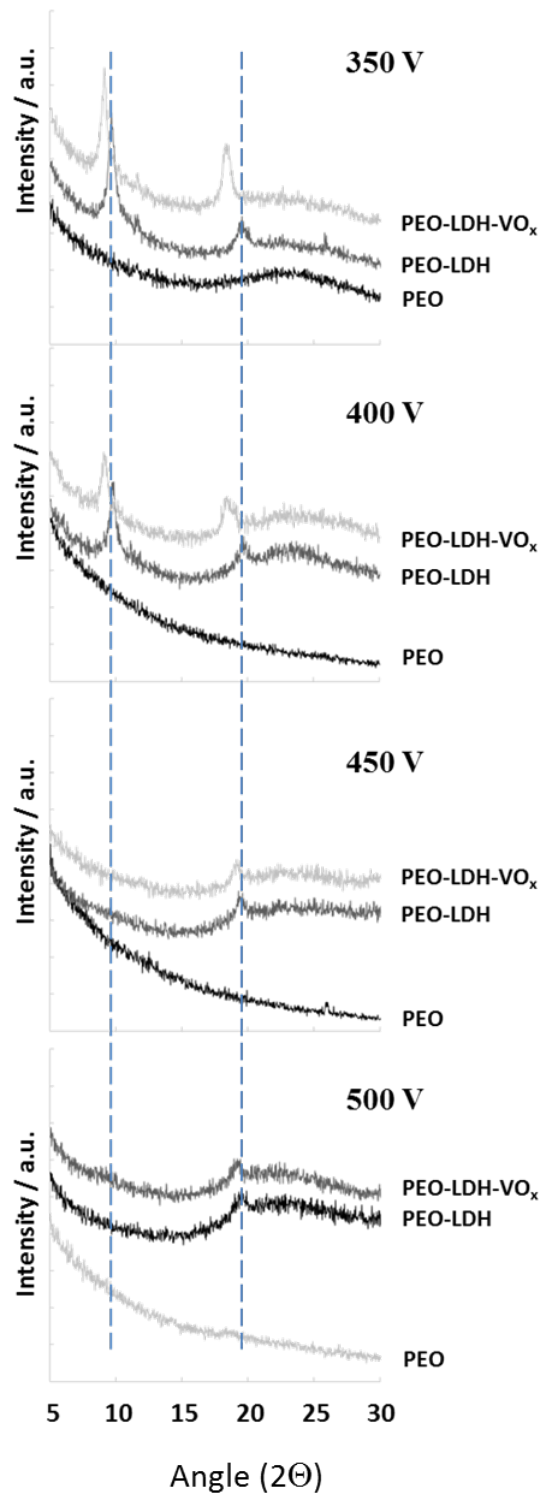
Figure 4

Three main regions are found on depth profiles of PEO coatings using GDOES (Fig. 5 a-d). The zone which contains silicon, phosphorus, aluminum and oxygen signals corresponds to the PEO layer (zone I). Additional elements (P and Si) confirm the incorporation of these elements from the electrolyte. Increased voltage leads to increased thickness of PEO coating

(Zone I). These results are in good agreement with the SEM cross-section measurements (Figure 1 b,d,f,h). There is an increase in aluminum and copper content simultaneously with a decrease of oxygen in a transition zone (zone II), which indicates where PEO coating and alloy substrate sputter at the same time. Transition from PEO coating (zone I) to the alloy (zone III) is not sharp due to the microroughness of the PEO/alloy interface after anodization. Zone III is characterized by the level of base alloy elements and a composition of the substrate.

After the growth of LDH-NO$_3$ GDOES results are similar to PEO coated sample (Fig. 5 e-h). Main difference in the LDH-NO$_3$ samples is zinc signal which is presented at the start of the sputtering. Appearance of zinc signal is associated with the formation of Zn-Al-NO$_3$ LDH on the surface of PEO. This signal is higher for PEO coatings prepared under lower voltages (Fig. 6), which agree with the planar view SEM images where higher amount of LDH flakes was found. In the case of PEO coatings prepared at a voltage of 450 V and 500 V the Zn signal is practically invisible (Fig. 6). This is in a good agreement with XRD measurements for these coatings. The same tendency as for zinc is observed in the case of the vanadium signal after the anion exchange reaction between nitrate and vanadate anions. It confirms that vanadate is associated with Zn-Al LDH structure and not only adsorbed on the surface (Fig. 5 i-l).
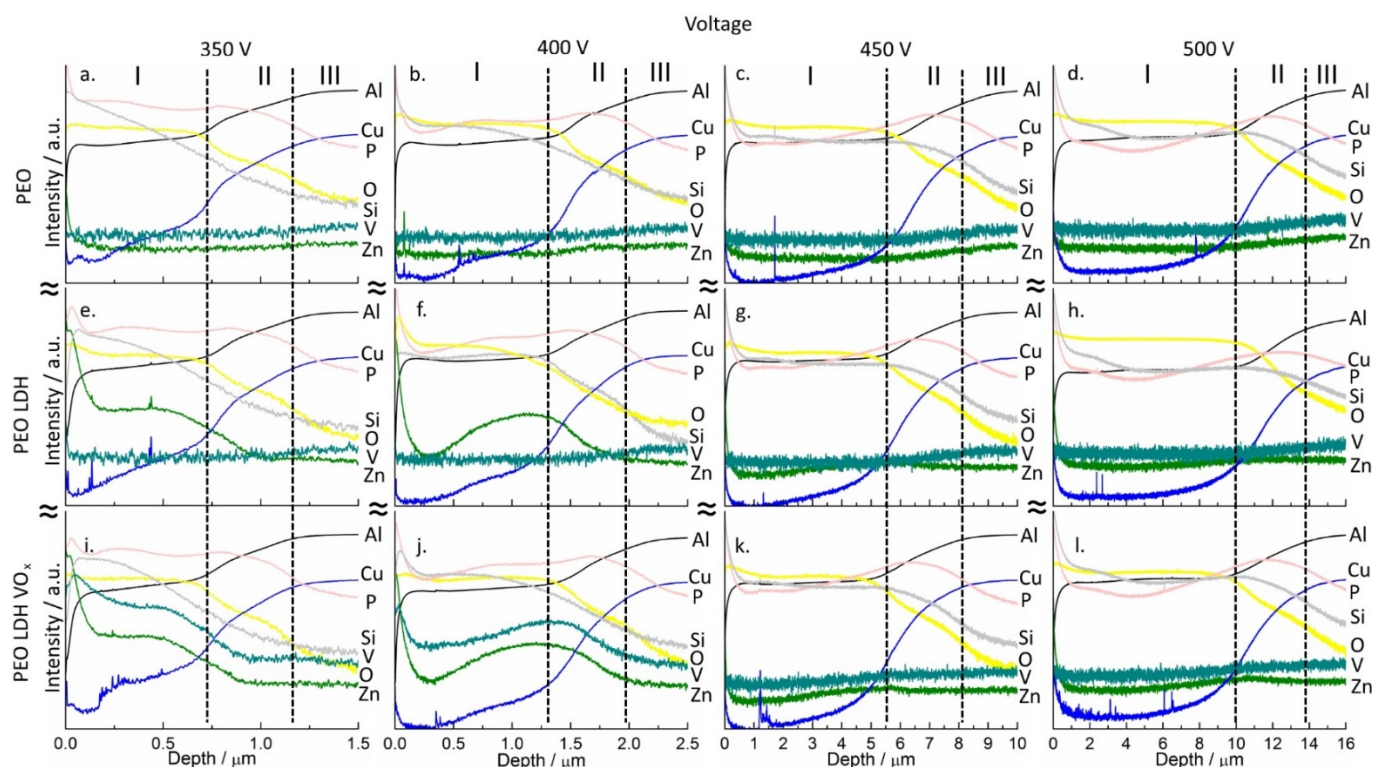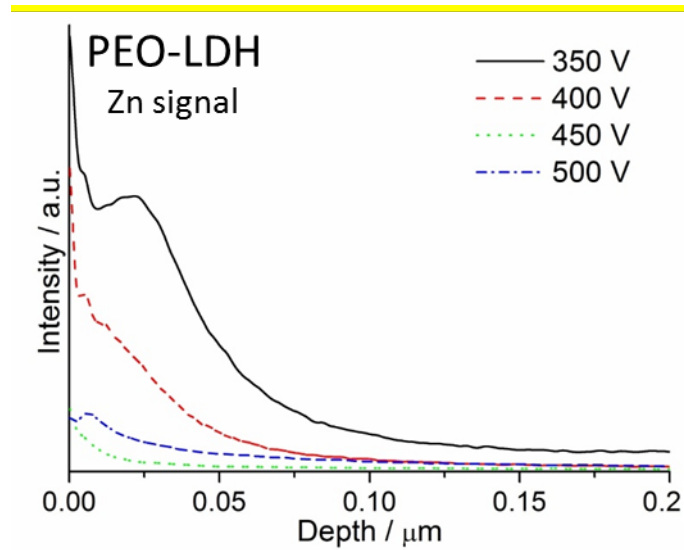
Figure 5

Figure 6

3.2. Electrochemical behavior

Electrochemical impedance spectroscopy was used to determine the integral effect of LDH formation and inhibitors incorporation on the corrosion behavior of the coatings. In order to compare the two most different conditions, Figures 7,8 depict the Bode plots for PEO-350 V and PEO-500 V with and without post-treatments up to 3 days of immersion in 0.5 wt.% NaCl solution at room temperature.

It is important to clarify that in this work the corrosion resistance of PEO layers is strongly associated with the individual characteristic of the coatings and therefore, with the final thickness. As it can be observed in the cross-sections of the coatings (Fig. 1), an increase in the voltage leads to thicker coatings with an increase of the impedance modulus up to two orders of magnitude from PEO-350 V to PEO-500 V (Fig. 7-8). From the point of view of protection, thicker coatings restrict the penetration of the electrolyte and therefore delay the corrosion process. However, in the particular case of PEO coatings, the effect of different processing parameter on the thickness of these layers, has been investigated and concluded that it is difficult to determine the optimum combination to obtain the best corrosion properties [41-43]. Some studies report that an increase in the thickness improves the corrosion properties of the PEO coated material due to an obstruction of the electrolyte permeation into the inner coating [48], while others report a decrease in the corrosion

14

properties of thicker layers due to the higher porosity of the ceramic coating, which is related to the nature of the micro-discharges during PEO process [49].

In frame of this study, the presence of different relaxation processes can be observed from the impedance spectra of the all PEO based coated specimens. The relaxation processes are difficult to distinguish in most of the cases due to a strong overlapping and they can be ascribed to: i) the time constant at high-frequency (10^3 Hz) is associated to the response of the porous part of the coating, which is clearer for the coating developed at 500 V ii) the middle frequency response of the system (10^1–10^2 Hz) can be attributed to the inner barrier layer of the PEO coating iii) the response of the electrochemical activities on the alloy surface can be attributed to the low-frequency time constant (0.1 Hz). For longer immersion times, all materials reveal the typical behavior for PEO coatings with a continuous decrease of low-frequency impedance modulus magnitude.

Different features can be observed from the interpretation of the impedance response. For the coatings formed at 350 V and after one hour of immersion, there is a clear beneficial effect of LDH-VO$_x$ on the corrosion resistance of PEO coatings showing higher modulus of the impedance at low frequencies (0.01 Hz) up to one order of magnitude. This effect is reduced for longer immersion times becoming insignificant after 3 days. The lowest value obtained for PEO-LDH after 1 h can be associated with a loss of the protective barrier properties of the coating during the formation of LDH under conditions described in the experimental part. The improvement after LDH-VO$_x$ post-treatment might be related to different factors including the total cover of the PEO-350 V surface with LDH flakes that obstruct the permeation of the electrolyte and the suppression of corrosion activity via release of vanadate.

For coatings developed under 500 V the beneficial effect of LDH and posterior intercalation of inhibitors is not that significant after 1 h of immersion. That is in agreement with the SEM analysis showing only a few flakes on the surface and as well with the GDOS studies that do not reveal a clear presence of these species. However, after 1 day of immersion there is an improvement of the corrosion resistance for PEO after post-treatments that might be associated with mass transfer limitation and diffusion resistance of the pores which contribute to the total impedance of the coated material. After 3 days of immersion the typical decrease of low-frequency impedance modulus magnitude is observed.

Using electrochemical impedance spectroscopy technique, it is not possible to clarify whether an active process in the PEO-based coating due to the presence of inhibitors species exists or not. With this aim, scanning vibrating electrode technique (SVET) was used to study the self-healing effect and validate the improvement of corrosion protection properties of formed coatings. Using SVET system, the monitoring of anodic and cathodic corrosion current densities in artificial micro-scale defects was performed (two artificial defects – 100 μm diameter and 20 μm depth with a distance of 1 mm between them – were drilled in the PEO-based samples).
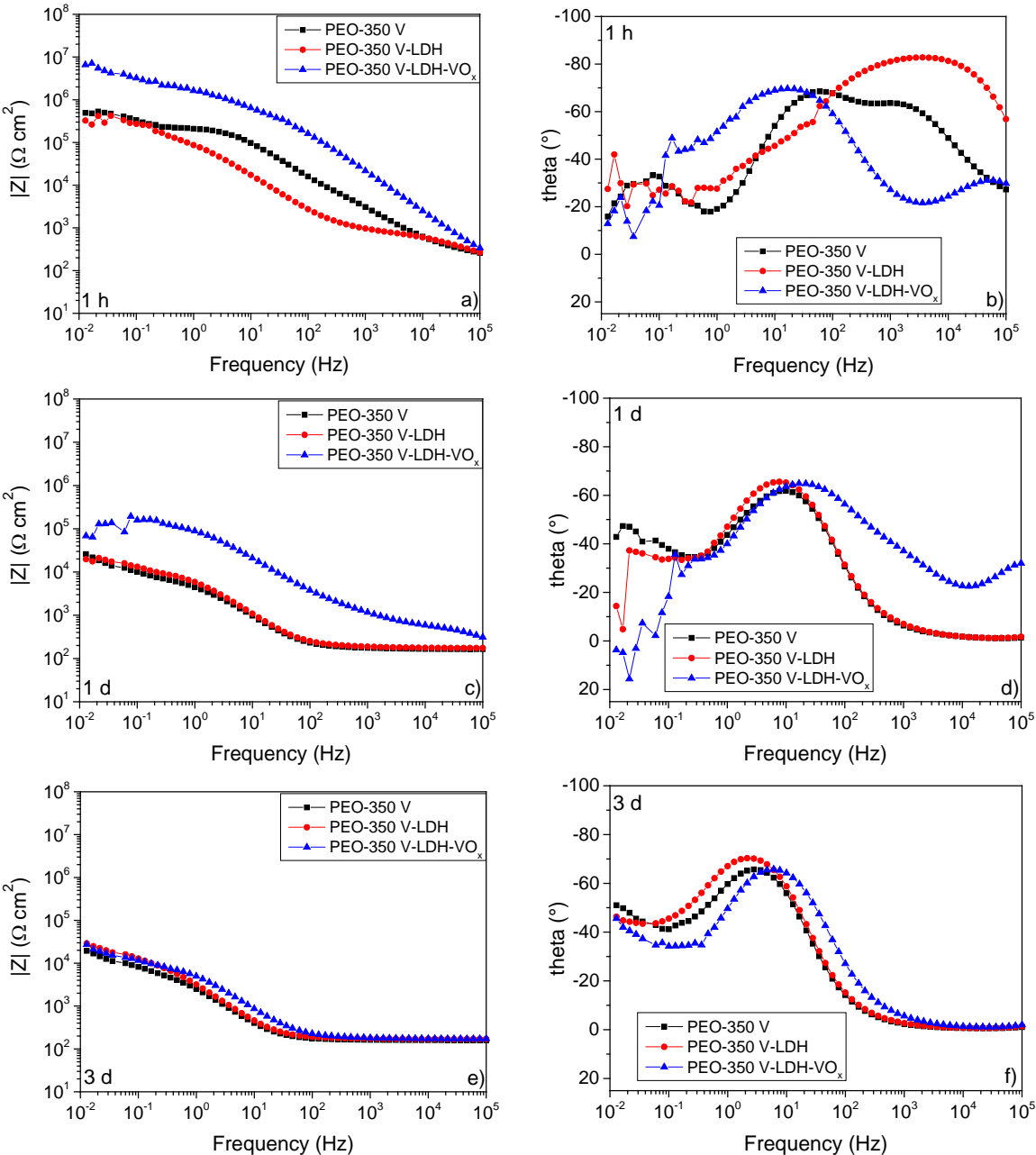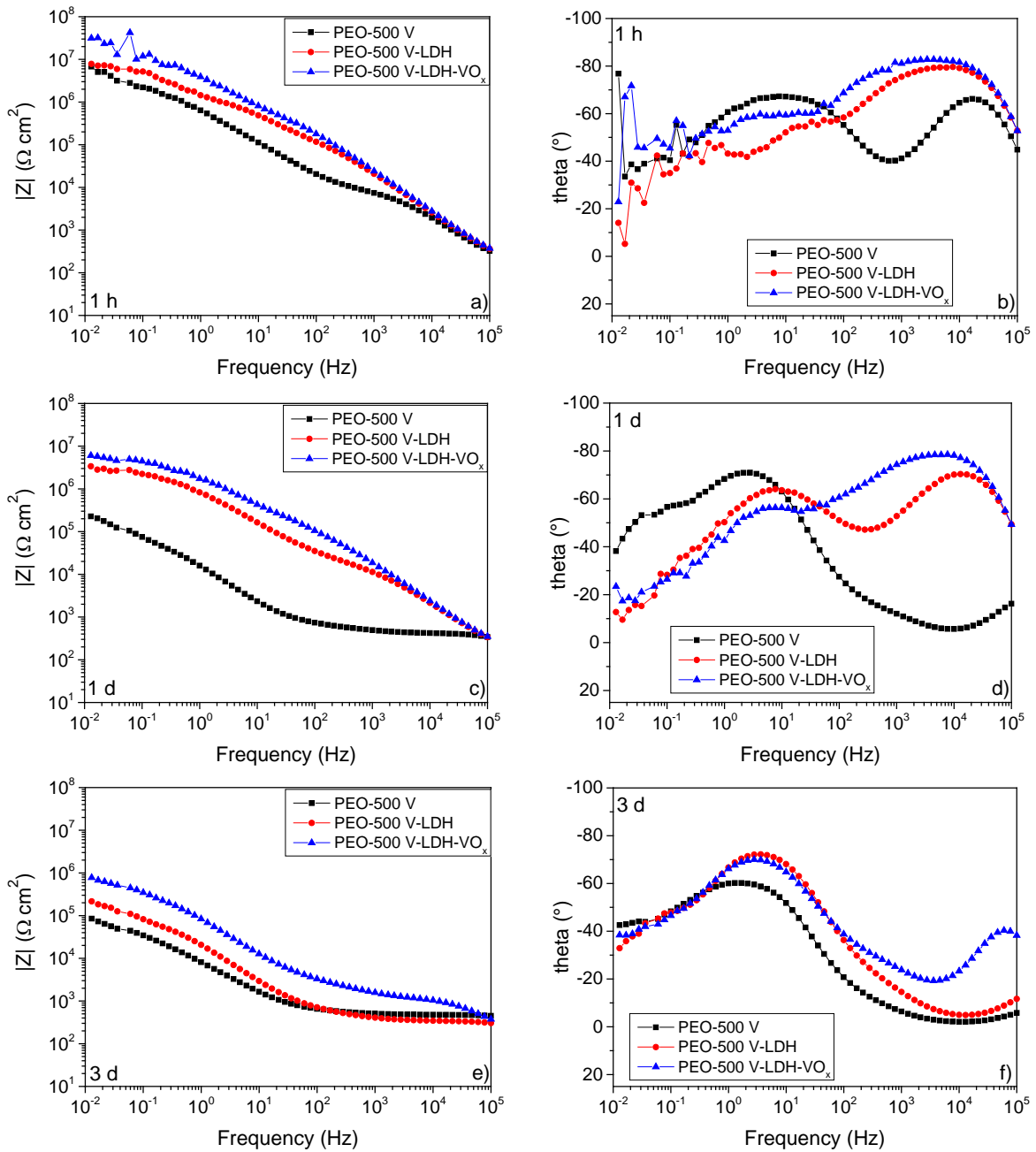

Figure 7

Figure 8

Figure 9 shows the microphotographs before the test and SVET maps taken in 0.05 M NaCl after 2 h, 10 h, and 22 hours for the original PEO (350 V and 500 V) coated AA2024 sample (a and d, respectively), PEO-LDH-NO$_3$ (b and e) and for PEO-LDH-VO$_x$ (c and f).

Strong corrosion activities are measured for the PEO-350 V coated AA2024 (Fig. 9 a). Corrosion starts not only at the places of drill defects but also in other locations confirming that barrier properties of PEO-350 V are very poor (the layer is extremely thin, as it was shown in Figure 1) and a sealing post-treatment is required.

17

As it was shown previously [30], metal dissolution leading to the cation flux is responsible for the anodic currents due to the reaction:

$$Al \rightarrow Al^{3+} + 3e \qquad\qquad [4]$$

The cathodic currents result from the following reaction of oxygen reduction:

$$O_2 + 2H_2O + 4e \rightarrow 4OH^- \qquad\qquad [5]$$

A significant delay in the appearance of corrosion activities is noted for the sample with PEO-350 V LDH-NO$_3$ and corrosion currents are detected only after 22 h of immersion. This behavior is related to the mechanism of corrosion protection with LDH: corrosive agent (Cl$^-$) and cathodically formed hydroxides (OH$^-$) are caught by LDH-NO$_3$ present at the surface. This leads to the deceleration of corrosion processes and low corrosion rate at the beginning of immersion.

The best corrosion protection performance was observed when vanadate as corrosion inhibitor was loaded into LDH nanocontainers (Figure 9-c). At the beginning of immersion, the low corrosion activity can be detected; however, after 22 h of immersion no corrosion activity was measured. This result confirms that LDH grown on PEO-350 V cover the surface and seal pores and vanadate acts as corrosion inhibitor for AA2024 as it was published previously for the bare [26] and pre-anodized AA2024 [30].

In comparison with PEO-350 V, PEO-500 V shows significantly stronger barrier protection that can be explained by higher thickness of the layer and lower accessibility of corrosive electrolyte to the substrate. Significantly lower corrosion activity was detected in the zones outside of artificial defects.

The distance between the SVET probe and the surface of the substrate can be the second reason of lower measured corrosion activity. In both cases the measurement was performed at average distance of 100 μm from the PEO surface. However, taking into account the own thickness of PEO-500 V layer (about 15 μm), the distance from the substrate surface increases up to about 115 μm. This change is significant for the SVET measurements and leads to the decrease of measured activity [50].

In frame of this work, SVET measurements for PEO-500 V LDH-VO$_x$ were performed under the same conditions as PEO-500 V and results can be compared. It can be seen, PEO-500 V LDH-VO$_x$ also performs the best corrosion protection and no signs of corrosion can be detected after 22 h of immersion.
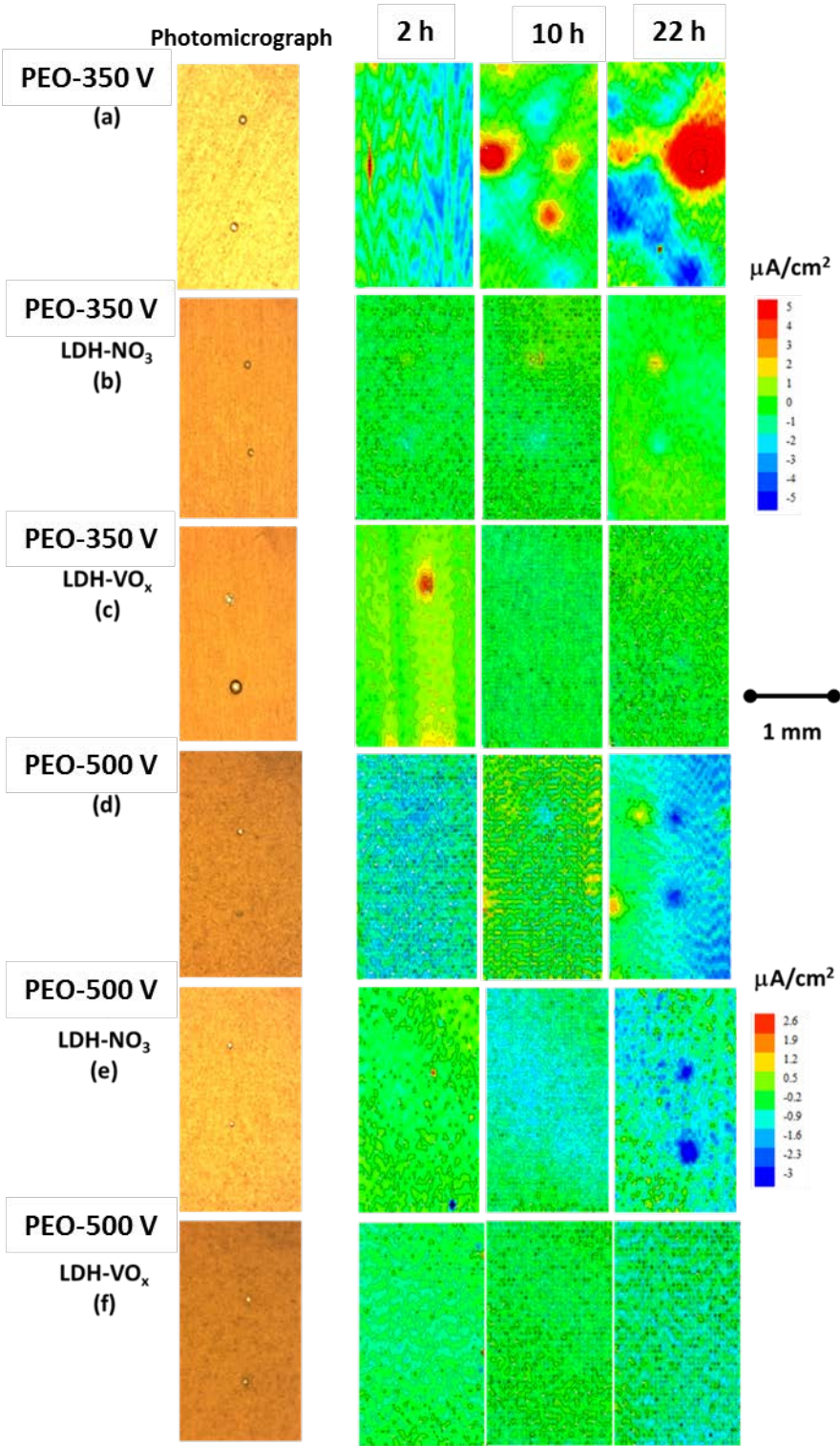

Figure 9

4. Conclusions

Four PEO coatings formed at different voltages (350, 400, 450, 500 V) were developed on AA2024 aluminum alloy showing a significant increase in thickness with voltage.

Zn–Al LDH layer was *in situ* grown and loaded with corrosion inhibitor (vanadate) on the coatings to provide active protection to the PEO layers.

Coatings formed at higher voltages (thicker and more stable) reveal a decrease of number of LDH flakes on the surface, as it is observed by SEM, XRD and GDEOS. This is mainly due to the mechanism of formation of LDH which strongly depends on the amount of $Al(OH)_2^+$ cations available from the material.

EIS technique shows better corrosion resistance for thicker coatings developed at higher voltages, but does not give information about the self-healing properties of the undamaged PEO layers.

SVET measurements reveal that the best corrosion protection performance is observed when vanadate as corrosion inhibitor was loaded into LDH nanocontainers.

References

1. B.L. Jiang, Y.M. Wang, Plasma electrolytic oxidation treatment of aluminium and titanium alloys, Surface Engineering of Light Alloys, Woodhead Publishing (2010) 110-154.
2. G. Sabatini, L. Ceschini, C. martini, J.A. Williams, I.M. Hutchings, Improving sliding and abrasive wear behaviour of as cast A356 and wrought AA7075 aluminium alloys by plasma electrolytic oxidation, Materials and Design, 31 (2010) 816-828.
3. A.L. Yerokhin, X. Nie, A. Leyland, A. Matthews, S.J. Dowey, Plasma electrolysis for surface engineering, Surface and Coatings Technology, 122 (1999) 73-93.
4. E. Matykina, R. Arrabal, P. Skeldon, G.E. Thompson, Investigation of the growth processes of coatings formed by AC plasma electrolytic oxidation of aluminium, Electrochimica Acta, 54 (2009) 6767-6778.
5. A. Lugovskoy, M. Zinigrad, A. Kossenko, B. Kazanski, Production of ceramic layers on aluminum alloys by plasma electrolytic oxidation in alkaline silicate electrolytes, Applied Surface Science, 264 (2013) 743-747.
6. Y. Cheng, J. Cao, M. Mao, H. Xie, P. Skeldon, Key factors determining the development of two morphologies of plasma electrolytic coatings on an Al–Cu–Li alloy in aluminate electrolytes, Surface and Coatings Technology, 291 (2016) 239-249.
7. A. Kossenko, M. ZInigrand, A universal electrolyte for the plasma electrolytic oxidation of aluminum and magnesium alloys, Materials and Design, 88 (2015) 302-309.
8. R.H.U. Khan, A. Yerokhin, X. Li, H. Dong, A. Matthews, Surface characterisation of DC plasma electrolytic oxidation treated 6082 aluminium alloy: Effect of current density and electrolyte concentration, Surface and Coatings Technology, 205 (2010) 1679-1688.
9. J. Martin, A. Melhem, I. Shchedrina, T. Duchanoy, A. Nominé, G. Henrion, T. Czerwiec, T. Belmonte, Effects of electrical parameters on plasma electrolytic oxidation of aluminium, Surface and Coatings Technology, 221 (2013) 70-76.
10. M. Mohedano, E. Matykina, R. Arrabal, B. Mingo, A. Pardo, PEO of pre-anodized Al–Si alloys: Corrosion properties and influence of sealings, Applied Surface Science, 346 (2015) 57-67.
11. M. Chen, S. Liu, J. Li, N. Cheng, X. Zhang, Improvement to corrosion resistance of MAO coated 2519 aluminum alloy by formation of polypropylene film on its surface, Surface and Coatings Technology, 232 (2013) 674-679.
12. S. Shrestha, A. Merstallinger, D. Sickert, B.D. Dunn, Preliminary evaluation of black coating on AA2219 alloy produced by plasma electrolytic oxidation (PEO) process for space applications, ISMSE (2003) 57-65.
13. K.A. Yasakau, J. Tedim, M.L. Zheludkevich, M.G.S. Ferreira, Smart self-healing coatings for corrosion protection of aluminium alloys, Handbook of Smart Coatings for Materials Protection (2014) 224-274.
14. M. Samadzadeh, S. Hatami Boura, M. Peikari, S.M. Kasiriha, A. Ashrafi, A review on self-healing coatings based on micro/nanocapsules, Progress in Organic Coatings, 68 (2010) 159-164.
15. D. Snihirova, S.V. Lamaka, M.F. Montemor, Smart composite coatings for corrosion protection of aluminium alloys in aerospace applications, Smart Composite Coatings and Membranes, (2016) 85-121.

16. I. Recloux, M. Mouanga, M. Druart, Y. Paint, M. Olivier, Silica mesoporous thin films as containers for benzotriazole for corrosion protection of 2024 aluminium alloys, Applied Surface Science, 346 (2015) 124-133.

17. A.S. Gnedenkov, S.L. Sinebryukhov, D.V. Mashtalyar, S.V. Gnedenkov, Localized corrosion of the Mg alloys with inhibitor-containing coatings: SVET and SIET studies Corrosion Science, 102 (2016) 269-278.

18. M. Mohedano, C. Blawert, M.L. Zheludkevich, "Cerium-based sealing of PEO coated AM50 magnesium alloy", Surface and Coatings Technology, 269 (2015) 145-154.

19. S.V. Oleinik, V.S. Rudnev, Yu.A.Kuzenkov, T.P. Yarovaya, L.F. Trubetskaya, P.M. Nedozorov, Corrosion inhibitors in PEO-coatings on aluminum alloys, Protection of Metals and Physical Chemistry of Surfaces, 50 (2014) 893-897

20. S.V. Oleinik, V.S. Rudnev, Yu.A.Kuzenkov, T.P. Yarovaya, L.F. Trubetskaya, P.M. Nedozorov, Modification of plasma electrolytic coatings on aluminum alloys with corrosion inhibitors, Protection of Metals and Physical Chemistry of Surfaces, 49 (2013) 885-890.

21. M. Sun, A. Yerokhin, M.Ya. Bychkova, D.V. Shtansky, E.A. Levashov, A. Matthews, Self-healing Plasma Electrolytic Oxidation Coatings Doped with Benzotriazole Loaded Halloysite Nanotubes on AM50 Magnesium Alloy, Corrosion Science, 111(2016) 753-769.

22. D. Grigoriev, Anticorrosion Coatings with Self-Recovering Ability Based on Damage-Triggered Micro- and Nanocontainers, Intelligent Coatings for Corrosion Control (2015) 283-333.

23. D.G. Shchkin, H. Mohwald, Surface-engineered nanocontainers for entrapment of corrosion inhibitors, Advanced Functional Materials, 17 (2007) 1451-1458.

24. D. Snihirova, S.V.Lamaka, M.F.Montemor, "SMART" protective ability of water based epoxy coatings loaded with CaCO3 microbeads impregnated with corrosion inhibitors applied on AA2024 substrates, Electrochimica Acta 83 (2012) 439-447.

25. M.L. Zheludkevich, R. Serra, M.F. Montemor, M.G.S. Ferreira, Oxide nanoparticle reservoirs for storage and prolonged release of the corrosion inhibitors, Electrochemistry. Communications 7 (2005) 836-840.

26. M.L. Zheludkevich, S.K. Poznyak, L.M. Rodrigues, D. Raps, T. Hack, L.F. Dick, T. Nunes, M.G.S. Ferreira, Active protection coatings with layered double hydroxide nanocontainers of corrosion inhibitor, Corrosion Science, 52 (2010) 602-611.

27. D. Scarpellini, C. Falconi, P. Gaudio, A. Mattoccia, P.G. Medaglia, A. Orsini, R. Pizzoferrato, M. Richetta, Morphology of Zn/Al layered double hydroxide nanosheets grown onto aluminum thin films, Microelectronic Engineering, 126 (2014) 129-133.

28. T. Hang, T. Truc, N. Duong, P. Vu, T. Hoang, reparation and characterization of nanocontainers of corrosion inhibitor based on layered double hydroxides, Applied Clay Science, 67 (2012) 18-25.

29. Y. Li, S. Li, Y. Zhang, M. Yu, J. Liu, Enhanced protective Zn–Al layered double hydroxide film fabricated on anodized 2198 aluminum alloy, Journal of Alloys and Compounds, 630 (2015) 29-36.

30. B. Kuznetsov, M. Serdechnova, J. Tedim, M. Starykevich, S. Kallip, M.P. Oliveira, T. Hack, S. Nixon, M.G.S. Ferreira, M.L. Zheludkevich, Sealing of tartaric sulphuric (TSA) anodized AA2024 with nanostructured LDH layers, RSC Adv., 6 (2016) 13942-13952.

31. D.E. Evans, R.C.T. Slade, Structural Aspects of Layered Double Hydroxides, Structure & Bonding, 119 (2005) 1-87.

32. M. Serdechnova, A.N. Salak, F.S. Barbosa, D.E.L. Vieira, J. Tedim, M.L. Zheludkevich, M.G.S. Ferreira, Interlayer intercalation and arrangement of 2-mercaptobenzothiazolate and 1,2,3-benzotriazolate anions in layered double hydroxides: in situ x-ray diffraction study, Journal of Solid State Chemistry, 233 (2016) 158-165.

33. J. Tedim, A. Kuznetsova, A.N. Salak, F. Montemor, D. Snihirova, M. Pilz, M.L. Zheludkevich, M.G.S. Ferreira Zn–Al layered double hydroxides as chloride nanotraps in active protective coatings, Corrosion Science, 55 (2012) 1-4.

34. M. Serdechnova, M. Mohedano, B. Kuznetsov, C.L. Mendis, M. Starykevich, S. Karpushenkov, J. Tedim, M.G.S. Ferreira, C. Blawert, M.L. Zheludkevich, PEO coatings with active protection based on in-situ formed LDH-nanocontainers. Journal of the Electrochemical Society 164 (2017) C36-C45.

35. T. Hashimoto, X. Zhang, X. Zhou, P. Skeldon, S.J. Haigh, G.E. Thompson, Investigation of dealloying of S phase (Al2CuMg) in AA 2024-T3 aluminium alloy using high resolution 2D and 3D electron imaging, Corrosion Science, 101 (2016), 157-164.

36. R.G. Buchheit, R.P. Grant, P.F. Halva, B. Mckenie, G.L. Zender, Local dissolution phenomena associated with S phase (Al2CuMg) particles in aluminium alloy 2024-T3, Journal of Electrochemical Society, 144 (1997) 2621-2628.

37. M. García-Rubio, M.P. de Lara, P. Ocon, S. Diekhoff, M. Beneke, A. Lavia, I. Garcia, Effect of postreatment on the corrosion behaviour of tartaric–sulphuric anodic films, Electrochimica Acta, 54 (2009) 4789-4800

38. J. Skykes, G.E. Thompson, D. Mayo, P. Skeldon, Anodic film formation on high stremgth aluminium alloy FVS0812, Journal of Materials Science 32 (1997) 4909-4916.

39. L.E. Fratila-Apachiei, F.D. Tichelaar, G. E. Thompson, H. Terryn, P. Skeldon, J. Duszczyk, L. Kathertman, A transmission electron microscopy study of hard anodic oxide layers on AlSi(Cu) alloys, Electrochimica Acta, 49 (2004) 3169-3177.

40. V. Dehnavi, X.Y. Liu, B.L. Luan, D.W. Shoesmith, S. Rohani, Phase transformation in plasma electrolytic oxidation coatings on 6061 aluminum alloy, Surface and Coatings Technology, 251 (2014) 106-114.

41. P. Bala Srinivasan, J. Liang, C. Blawert, M. Störmer, W. Dietzel, Effect of current density on the microstructure and corrosion behaviour of plasma electrolytic oxidation treated AM50 magnesium alloy, Applied Surface Science, 255 (2009) 4212-4218.

42. J. Xu, F. Liu, J.Luo, L.Zhao, Effects of Anodic Voltages on Microstructure and Properties of Plasma Electrolytic Oxidation Coatings on Biomedical NiTi Alloy, Journal of Materials Science & Technology, 29 (2013) 22-28.

43. W. Zhu, Y. Fang, H. Zheng, G. Tan, H. Cheng, C.Ning, Effect of applied voltage on phase components of composite coatings prepared by micro-arc oxidation, Thin Solid Films, 544 (2013) 79-82.

44. X. Lu, C. Blawert, Y. Huang, H. Ovri, M.L. Zheludkevich, K.U. Kainer, Plasma electrolytic oxidation coatings on Mg alloy with addition of SiO2 particles, Electrochimica Acta, 187 (2016) 20-33.

45. T. Galvão; C. Neves; A. Caetano; F. Maia; D. Mata; E. Malheiro; M. Ferreira; A. Bastos; A. Salak; J. Gomes; J. Tedim; M.G.S. Ferreira, Control of Crystallite and Particle Size in the Synthesis of Layered Double Hydroxides: Macromolecular Insights and a Complementary Modelling Tool, Journal of Colloid and Interface Science, 468 (2016) 86–94.

46. E. L. Cussler, Diffusion: mass transfer in fluid systems, Cambridge university press (2009) 647.

47. J. Tedim, M.L. Zheludkevich, A.C. Bastos, A.N. Salak, A.D. Lisenkov, M.G.S. Ferreira, Influence of preparation conditions of Layered Double Hydroxide conversion films on corrosion protection, Electrochimica Acta, 117 (2014) 164-171.

48. Y. Gao, A. Yerokhin, A.Matthews, Effect of current mode on PEO treatment of magnesium in Ca- and P-containing electrolyte and resulting coatings, Applied Surface Science, 316 (2014) 558-567.

49. G. Rapheal, S. Kumar, N. Scharnagl, C. Blawert, Effect of current density on the microstructure and corrosion properties of plasma electrolytic oxidation (PEO) coatings on AM50 Mg alloy produced in an electrolyte containing clay additives, Surface and Coatings Technology, 289 (2016) 150-164.

50. O. Dolgikh, A.S. Demeter, S.V. Lamaka, M. Taryba, A.C. Bastos, M.C. Quevedo, J. Deconinck, Simulation of the role of vibration on Scanning Vibrating Electrode Technique measurements close to a disc in plane, Electrochimica Acta, 203 (2016) 379-387.

Figure captions

Figure 1. Secondary electron images of the coatings plan view and cross section: (a,b) PEO-350 V, (c,d) PEO-400 V, (e,f) PEO-450 V, (g,h) PEO-500 V.

Figure 2. Secondary electron images of the coatings plan view before and after LDH-NO3 formation: (a) PEO-350 V, (b) PEO-350 V-LDH-NO$_3$, (c) PEO-400 V, (d) PEO-400 V-LDH, (e) PEO-450 V, (f) PEO-450 V-LDH, (g) PEO-500 V, (h) PEO-500 V-LDH.

Figure 3. XRD patterns of PEO coated AA2024 at different voltages (350 V-500 V).

Figure 4. XRD patterns of PEO coated AA2024 at different voltages (350 V-500 V), covered with LDH before (LDH-NO$_3$) and after inhibitor intercalation (LDH-VO$_x$)

Figure 5. Qualitative depth profile measured by GDOES of PEO coated AA2024 at different voltages (350 V-500 V), covered with LDH before (LDH-NO$_3$) and after inhibitor intercalation (LDH-VO$_x$).

Figure 6. GDOES zinc signal profile for different PEO coatings (350 V-500 V) after LDH treatment.

Figure 7. Electrochemical impedance spectroscopy measurements (bode plots) for PEO-350 V before and after post-treatments (LDH and LDH-VO$_x$) after immersion in 0.5 wt.% NaCl: (a,b) 1 h (c,d) 1 d (e,f) 3 d.

Figure 8. Electrochemical impedance spectroscopy measurements (bode plots) for PEO-500 V before and after post-treatments (LDH and LDH-VO$_x$) after immersion in 0.5 wt.% NaCl: (a,b) 1 h (c,d) 1 d (e,f) 3 d.

Figure 9. Microphotographs before immersion in 0.05 M NaCl and SVET maps after immersion in 0.05 M NaCl after 2 h, 10 h, and 22 hours for: (a)PEO-350V, (b) PEO-350V-LDH, (c) PEO-350V-VO$_x$, (d) PEO-500V-LDH, (e) PEO-500V-LDH, (f) PEO-500V-VO$_x$.